JMEPEG (2018) 27:5709–5717
https://doi.org/10.1007/s11665-018-3678-y

1059-9495/$19.00

Effect of Minor Er on the Microstructure and Properties of Al-6.0Mg-0.4Mn-0.1Cr-0.1Zr Alloys

Hailong Chen, Tianfu Yu, Zhongyuan Qi, Ruizhi Wu, Guojun Wang, Xinyu Lv, Fuguan Cong, Legan Hou, Jinghuai Zhang, and Milin Zhang

(Submitted April 19, 2018; in revised form July 25, 2018; published online October 1, 2018)

As-cast Al-6.0Mg-0.4Mn-0.1Cr-0.1Zr alloys containing different additions of Er were prepared. Then, the specimens were carried out homogenization heat treatment, hot rolling, cold rolling, and annealing. The effects of minor Er on the microstructure and properties of Al-6.0Mg-0.4Mn-0.1Cr-0.1Zr alloy were investigated. Results show that addition of Er can refine the microstructure and improve the mechanical properties of the alloys. As for the annealed alloys, the addition of 0.33%Er can increase the tensile strength by 29 MPa. Strength increment is mainly attributed to refinement and the precipitation of Al_3Er and $Al_3(Er, Zr)$. Additionally, the minor Er can improve the corrosion resistance of the alloys, which can be attributed to the compact composite oxide film of Er-O and Al-O, purification, and modification.

Keywords Al-Mg-Mn alloy, erbium, refinement, rolling, strength

1. Introduction

Aluminum alloys possess properties of high strength, corrosion resistance, and lightweight. Accordingly, they become a kind of popular engineering metallic materials (Ref 1-3). Al-Mg-based alloys possess many interesting properties, such as good weldability, good corrosion resistance, high strength, and good formability. They offer the best combination of strength and corrosion resistance among all the series of aluminum alloy. Accordingly, Al-Mg-based alloys become the excellent candidates in the applications of shipbuilding, cryogenic vessels, automotive body, and trains (Ref 4).

Hailong Chen, College of Shipbuilding Engineering, Harbin Engineering University, Harbin 150001, People's Republic of China; **Tianfu Yu, Legan Hou,** and **Jinghuai Zhang**, Key Laboratory of Superlight Materials and Surface Technology, Ministry of Education, Harbin Engineering University, Harbin 150001, People's Republic of China; **Zhongyuan Qi**, Key Laboratory of Superlight Materials and Surface Technology, Ministry of Education, Harbin Engineering University, Harbin 150001, People's Republic of China; and Suzhou Changfeng Avionics Co., LTD., Suzhou 215151, People's Republic of China; **Ruizhi Wu**, Key Laboratory of Superlight Materials and Surface Technology, Ministry of Education, Harbin Engineering University, Harbin 150001, People's Republic of China; College of Science, Heihe University, Heihe 164300, People's Republic of China; and Key Laboratory of Lightweight and High Strength Structural Materials of Jiangxi Province, Nanchang University, Nanchang 330031, People's Republic of China; **Guojun Wang, Xinyu Lv,** and **Fuguan Cong**, Northeast Light Alloy Co., Ltd, Harbin 150060, People's Republic of China; and **Milin Zhang**, Key Laboratory of Superlight Materials and Surface Technology, Ministry of Education, Harbin Engineering University, Harbin 150001, People's Republic of China; and College of Science, Heihe University, Heihe 164300, People's Republic of China. Contact e-mails: Ruizhiwu2006@yahoo.com and rzwu@hrbeu.edu.cn.

Al-Mg-based alloys belong to non-heat-treatable alloys. The strengthening of the alloys is mainly caused by refinement and secondary phases. One of the effective ways to improve properties of aluminum alloys is microalloying with transition metals or rare earth metals, such as Sc and Zr (Ref 5-7). The additions of Sc and/or Zr bring about the secondary phases of Al_3Sc, Al_3Zr, and $Al_3(Sc,Zr)$, which cause the secondary-phase strengthening and retard recrystallization (Ref 8). However, the addition of Sc entails a very high cost. As a suitable substitution for Sc, minor Er can also obviously improve the strength and ductility of aluminum alloys. In Al-Zr binary alloy, Er dissolves into Al_3Zr phase by replacing some Zr, forming $Al_3(Er, Zr)$ precipitations (Ref 9, 10). However, in the complicated alloy system, the existence form and strengthening mechanism of minor Er still remain unclear.

The purpose of this work was to investigate the effects of minor Er on the refinement and dispersive precipitation in Al-6.0Mg-0.4Mn-0.1Cr-0.1Zr-(0-0.45)Er. The microstructure, mechanical properties, and corrosion resistance of the alloys under different processing states were researched.

2. Experimental Procedures

Commercial pure Al (99.8 wt.%), commercial pure Mg (99.5 wt.%), and master alloys of Al-10Mn, Al-6Er, Al-3Cr, and Al-5Zr were used to prepare alloys. The materials were loaded in a crucible and melted in an electric resistance furnace at 760 °C. The melt was cast into a permanent mold at 730 °C. The nominal and actual compositions of the alloys are listed in Table 1. The as-cast ingots were homogenized at 490 °C for 24 h. After homogenization, the ingots were machined with the dimensions of 25 mm × 50 mm × 160 mm, and the as-received plates were hot-rolled at 430 °C with a thickness reduction from 25 to 5 mm, the reduction ratio of single rolling pass of 25%, and the total reduction ratio of 80%. The hot-rolled specimens were annealed at 375 °C for 2 h before cold rolling. During the cold rolling, the reduction ratio of single rolling pass is 30% and the total reduction ratio is 60%. After

Table 1 The nominal and actual compositions of the investigated alloys (wt.%)

Alloys	Mg	Mn	Cr	Zr	Er	Al
Al-6.0Mg-0.4Mn-0.1Cr-0.1Zr	6.02	0.44	0.13	0.12	0	Balance
Al-6.0Mg-0.4Mn-0.1Cr-0.1Zr-0.15Er	5.91	0.43	0.12	0.13	0.21	Balance
Al-6.0Mg-0.4Mn-0.1Cr-0.1Zr-0.33Er	6.08	0.40	0.12	0.14	0.32	Balance
Al-6.0Mg-0.4Mn-0.1Cr-0.1Zr-0.45Er	6.09	0.42	0.12	0.14	0.39	Balance

cold rolling, the final thickness of the sheets is 2 mm. Finally, as-rolled sheets were stabilizing annealed at 250 °C for 2 h.

The microstructure was observed with optical microscopy (OM), scanning electron microscopy (SEM), and transmission electron microscopy (TEM). Before OM and SEM observation, the specimens were etched in a solution of HNO_3+HCl+HF. The elemental compositions were analyzed with an energy-dispersive spectrometer (EDS). The phase compositions were measured with x-ray diffraction (XRD).

Tensile testing was performed at room temperature. The tensile direction was parallel to the rolling direction, and the initial strain rate was 1.0×10^{-3} s^{-1}. Vickers hardness measurements were taken with a load of 50 kgf and a dwell time of 15 s.

The 3.5% NaCl aqueous solution and a standard three-electrode configuration were used in electrochemical measurements. A saturated calomel electrode served as the reference electrode, a platinum plate served as the counter electrode, and the sample served as the working electrode. The scanning rate was 2 mV/s. The intergranular corrosion was measured according to the standard of GB/T7998-2005. The specimens for intergranular corrosion measurement were etched in 7.5% NaOH aqueous solution at 60 °C for 3 min. Then, they were desmutted in 65% HNO_3 for 1 min and were immersed in a mixed solution of 30 g/L NaCl and 10 ml/L HCl for 24 h. Finally, the corroded microstructure was observed with OM.

3. Results

3.1 Microstructure of As-Cast Alloys

Figure 1 shows the OM images of the as-cast alloys with different Er contents. All the specimens show a dendritic structure. The alloy without Er presents the coarse microstructure, as shown in Fig. 1(a). The addition of 0.15 wt.% Er does not result in obvious refinement, as shown in Fig. 1(b). With addition of 0.33 wt.% Er, the microstructure is refined significantly, as shown in Fig. 1(c). Further increase of Er only leads to a slight refinement, as shown in Fig. 1(d).

XRD patterns of the as-cast alloys without Er and with 0.33 wt.% Er are shown in Fig. 2. It can be found that Al_6Mn and Al_3Mg_2 exist in the as-cast alloys. In the alloy with 0.33 wt.% Er, there also exists Al_3Er phase.

Figure 3 shows SEM images and EDS patterns for the precipitations of the as-cast alloys with different Er contents. In Fig. 3(a), there exist long-strip Al_6Mn phase and block-like Al_3Mg_2 phase (Ref 11). In the alloy with 0.33 wt.% Er, there exist some dispersive particles, denoted as 3 in Fig. 3(b). Figure 3(d) shows the EDS patterns for the particles in Fig. 3(b), indicating that the particle is an intermetallic compound containing Al and Er. Combined with the patterns of XRD, the compound can be deduced to be Al_3Er that is formed from eutectic reaction (Ref 12). When Er content is 0.45 wt.%, the size of Al_6Mn and Al_3Mg_2 decreases. The addition of Er reduces the solubility of Mn and Mg, and the segregated Mn and Mg form compounds with Al, denoted as 4 in Fig. 3(c). The amount of Al_3Er increases, denoted as 5 in Fig. 3(c).

Figure 4 shows TEM images of the as-cast alloy with 0.33 wt.% Er. Al-Mn phases exist in the matrix in various forms. The rhombic and long-strip Al-Mn phases are pointed out in Fig. 4(a). Liu et al. (Ref 13) reported that the Mn atoms of Al_6Mn are partially replaced by Fe atoms, causing the formation of $Al_6(Mn,Fe)$. Some nanoscale primary phases exist at the grain boundary, as shown in Fig. 4(b). During solidification process, Er reacts with Al to form primary Al_3Er particles (Ref 14). The diameter of primary Al_3Er particles is about 70-110 nm.

3.2 Microstructure of Homogenized Alloys

Figure 5 shows the OM images of the alloys after homogenization at 490 °C for 24 h. During homogenization, atoms diffuse by thermal vibration. The alloying elements segregate at dendrite boundaries, and the precipitations with low melting points are dissolved into matrix, causing dendrite boundary depletion. Compared with the alloy without Er, the alloy with 0.15 wt.% Er is refined obviously, as shown in Fig. 5(b). With the addition of 0.33 wt.% Er and 0.45 wt.% Er, the microstructure is further obviously refined and the dendritic structure disappears.

SEM image of the homogenized alloy without Er is shown in Fig. 6. The amount of non-equilibrium phase decreases significantly. There only exists a small amount of undissolved Al_3Mg_2 phase into the matrix.

Figure 7 shows TEM images and EDS patterns for the precipitations of the homogenized alloy with 0.33 wt.% Er. The precipitations are indicated by arrows in Fig. 7(a), (b), and (c) shows the EDS patterns for the marked particles in Fig. 7(a). According to EDS results, the precipitations indicated by arrow 1 are array of secondary Al_3Er. The diameter of secondary Al_3Er particles is about 20 nm, which is smaller than the primary Al_3Er. In the magnified observation of the specimen, it can be found that there are some other precipitations in the alloy, indicated by arrows 2 in Fig. 7(b). Compared with the secondary Al_3Er, these precipitates have a shell-like structure with a smaller size, about 6-8 nm. Wen et al. (Ref 15) reported that this kind of shell-like particle is $Al_3(Er,Zr)$, which possesses a smaller size than the secondary Al_3Er. The secondary Al_3Er and $Al_3(Er,Zr)$ are both $L1_2$ structure. In the phase of $Al_3(Er,Zr)$, Zr segregates at the surface of a core of Al_3Er to form a core–shell structure.

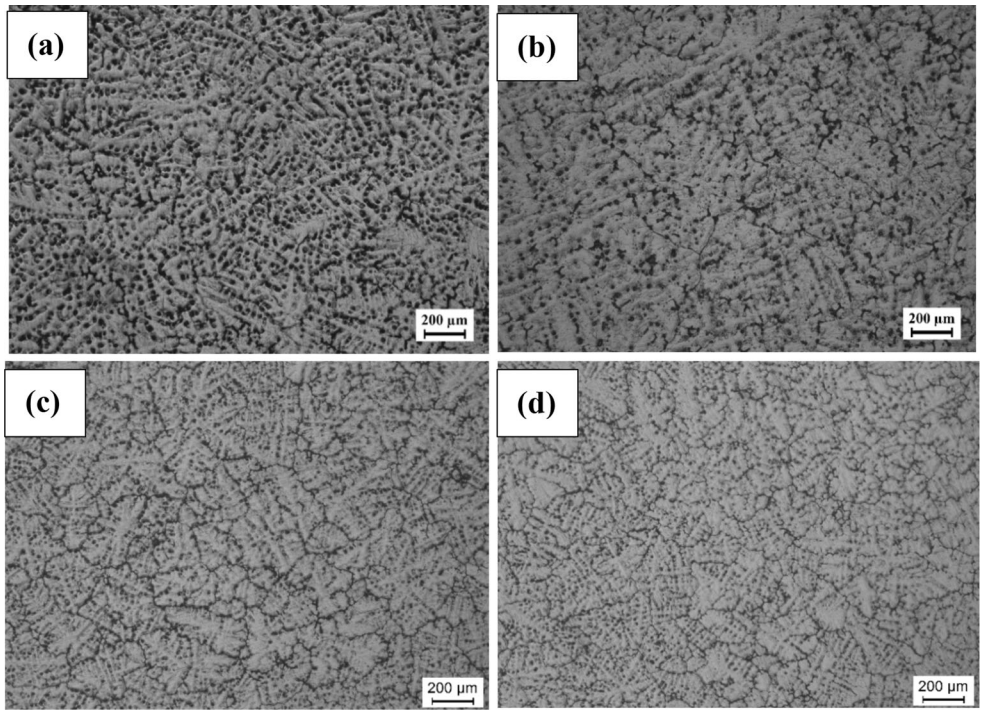

Fig. 1 OM of as-cast alloys (a) without Er, (b) 0.15 wt.% Er, (c) 0.33 wt.% Er, (d) 0.45 wt.% Er

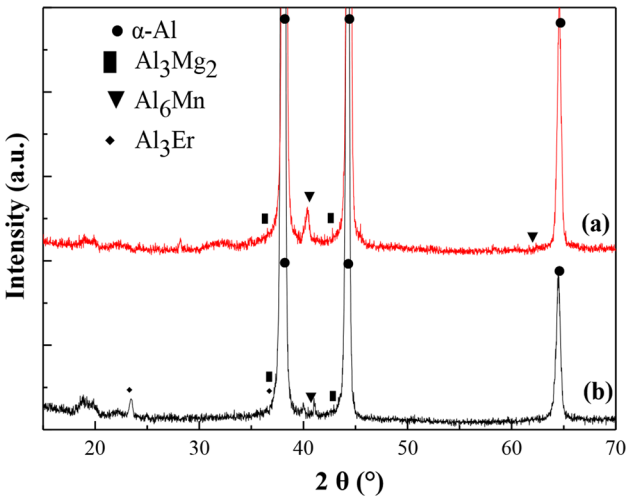

Fig. 2 XRD patterns of as-cast alloys. (a) Without Er, (b) 0.33 wt.% Er

3.3 Microstructure of Annealed Alloys After Rolling

Figure 8 shows TEM images of the alloy with 0.33 wt.% Er after annealing at 250 °C for 2 h. During cold rolling, a great amount of dislocations entangle together with a high dislocation density. During annealing, the entangled dislocations begin to move to form a dislocation network, as shown in Fig. 8(a). It indicates that the alloy is in the recovery stage. At the same time, sub-grains form in the alloy, as shown in Fig. 8(b), which is the result of dislocation motion. Figure 8(c) shows that Al_3Er and $Al_3(Er, Zr)$ particles pin the dislocations.

3.4 Mechanical Properties of the Alloys

Figure 9 shows the hardness of the alloys under different states. The addition of Er obviously improves the hardness of the alloys. Under the states of as-cast, homogenization, and hot rolling, the hardness values of the alloys increase with Er content. Compared with the hot-rolled alloy without Er, the hardness of the hot-rolled alloy with 0.45 wt.% Er increases by 30%. Under the states of cold rolling and annealing, with addition of 0.45 wt.% Er, the hardness is reduced compared with that of the alloy with 0.33 wt.% Er. It indicates that excessive addition of Er leads to degradation of mechanical properties. After stabilizing annealed at 250 °C, the deformation energy of the alloys is released, causing the decrease in hardness.

Tensile properties of the alloys after annealing at 250 °C for 2 h are listed in Table 2. The results show that strength increases with Er content. The tensile strength of the alloy with 0.33 wt.% Er is 461, 30 MPa higher than that of the alloy without Er. With the addition of 0.45 wt.% Er, the strength decreases. The mechanical properties of the alloy deteriorate because of excessive erbium.

3.5 Corrosion Properties of the Alloys After Annealing

The corrosion potential and corrosion current density of the alloys are compared in Tafel polar curves, as shown in Fig. 10. With the increment of Er content, the corrosion current density decreases, and the corrosion potential increases. With addition of 0.45 wt.% Er, the corrosion potential is the largest, − 1.118 V, and the corrosion current density is 5.182×10^{-6} A cm^{-2}.

Figure 11 shows the typical cross-sectional corrosion microstructure, in which the corresponding maximum corro-

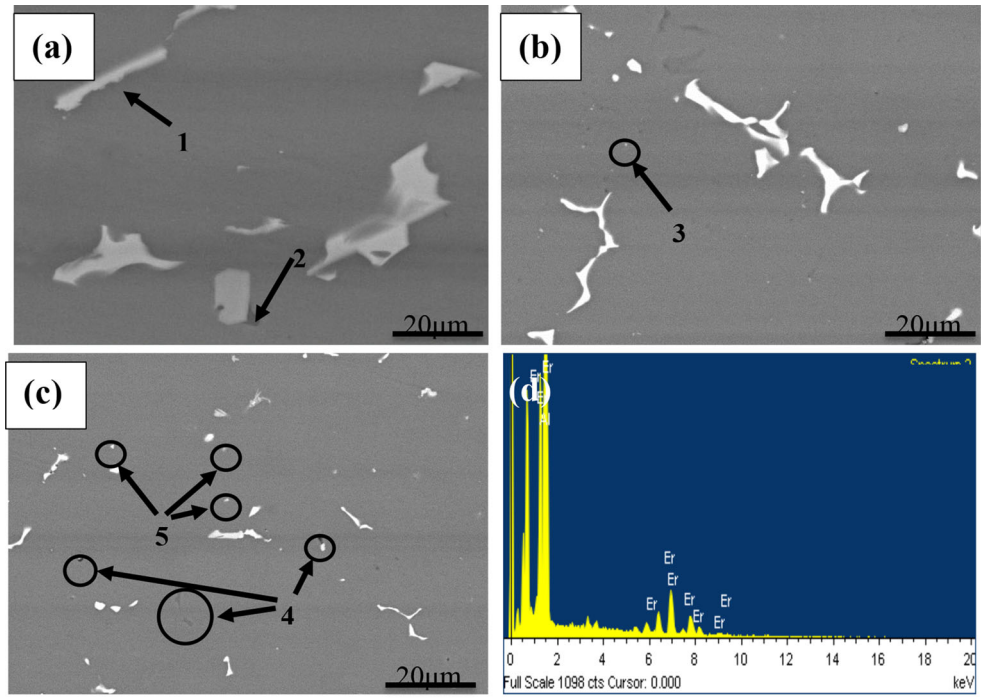

Fig. 3 SEM and EDS for the precipitations of as-cast alloys with different Er contents: (a) without Er, (b) 0.33 wt.% Er, (c) 0.45 wt.% Er, (d) EDS pattern of marked particle in (b)

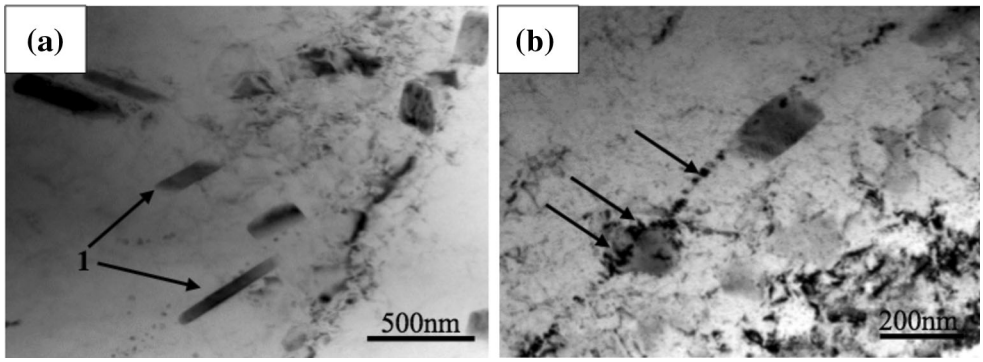

Fig. 4 TEM images of the as-cast alloy with 0.33 wt.% Er: (a) Al-Mn phases, (b) primary Al_3Er

sion depths of the annealed alloys are provided. The alloys have different intergranular corrosion susceptibility. The maximum corrosion depth decreases with the increase in Er content, indicating the improvement in intergranular corrosion resistance.

4. Discussions

4.1 The Behavior of Er in As-Cast and Homogenized Alloys

The refinement mechanism of Er in the alloys can be attributed to two factors: constitutional supercooling and heterogeneous nucleation.

During solidification, α-Al nucleates first near the mold wall and grows inwards to form dendrites. Supersaturated Er atoms are expelled from the dendrites and accumulate at the front of the interface between solid and liquid. Al-Er binary phase diagram shows that Er reacts with Al to form primary Al_3Er when the temperature reaches the eutectic temperature. When the nucleation of α-Al in the melt is enough, the primary Al_3Er is adsorbed on the α-Al nucleations. Ji et al (Ref 16) reported that, after adding 0.7 wt.% Er in Al-5Mg alloy, the degree of supercooling increases by 37 °C. The redistribution of supersaturated Er causes the variation of the solute concentration in the front of the solid–liquid interface, changing the solidification temperature gradient and causing a constitutional supercooling. As a result, the crystallization of cellular dendrites is

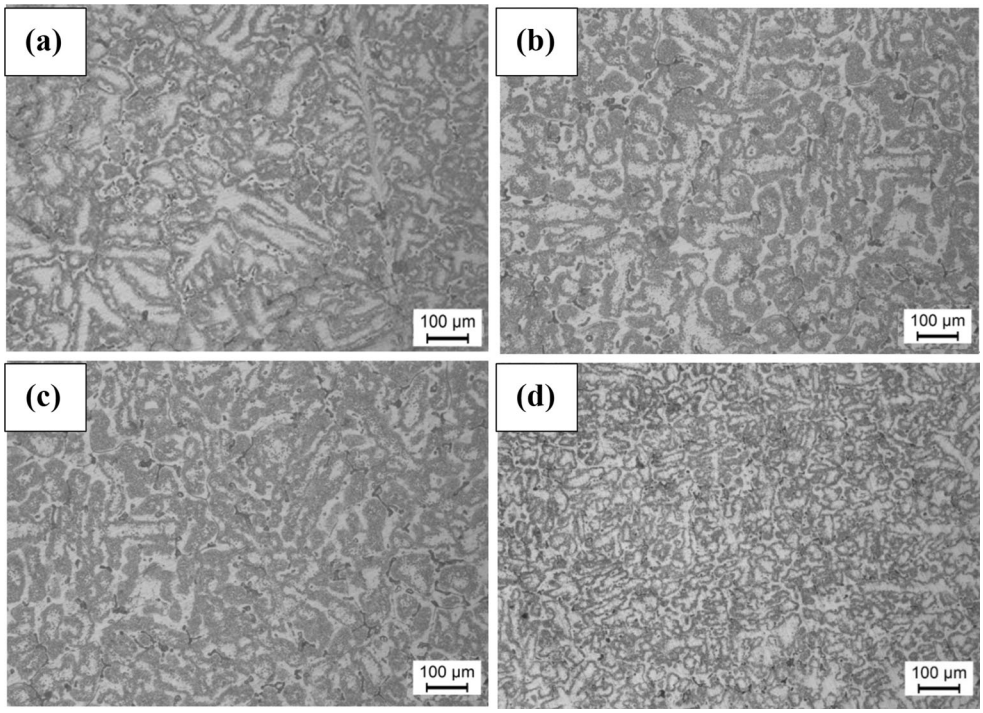

Fig. 5 OM images of as-homogenized alloys (a) without Er, (b) 0.15 wt.% Er, (c) 0.33 wt.% Er, (d) 0.45 wt.% Er

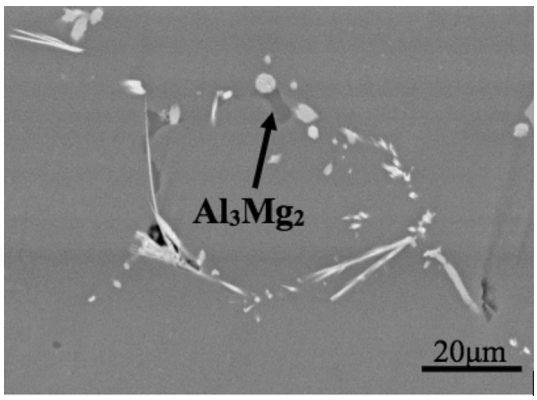

Fig. 6 SEM image of the alloy without Er homogenized at 490 °C for 24 h

intense, and a denser dendrite structure is formed (Ref 17). With the increment of Er content, the number of secondary dendrite increases, and finally, the dendrite spacing decreases.

Jones and Humphreys (Ref 18) reported that, in the process of cooling and solidification, the particles served as the core of heterogeneous crystal nucleus should meet three requirements: The particles should have a common interface with the substrate, and the arrangement of atoms on the interface is similar, and the lattice mismatch does not exceed 5%; the particles possess a high melting point; the particle should be the primary precipitated phase. The primary Al_3Er compound meets all the above requirements. The effectiveness of the nuclei depends on the relationships between the lattice types and parameters of the particle and α(Al) matrix. The similarity in lattice types plays an important role in refining (Ref 19, 20). Al_3Er particles have good coherent relationship with the aluminum matrix. The mismatch between the Al_3Er particles and the aluminum matrix is 4.08%. Al_3Er particles have a high melting point and stability in the molten liquid. Therefore, Al_3Er satisfies the lattice matching principle and can serve as a good nucleating agent.

$L1_2$-structured Al_3Er particles accumulate at the front of the interface between solid and liquid. The surface of the particles can be wetted by liquid phase easily. The liquid around the particles can form a new nucleus on the surface of segregated Al_3Er particles. There are many smaller dendrites around the large dendrites in Fig. 1(c) and (d). The nucleation rate is improved, and the microstructure of as-cast alloy is refined.

During homogenization, alloying elements that segregate at dendrite boundaries and the precipitations with low melting points are dissolved into matrix. With the temperature decreasing, secondary Al_3Er and $Al_3(Er, Zr)$ precipitate from the solid solution. Accordingly, there are three kinds of formation of Er in alloy, a part of Er dissolved into Al matrix, primary Al_3Er, and secondary Al_3Er and $Al_3(Er, Zr)$.

4.2 Mechanical and Corrosion Properties Improvement

Under the states of as-cast and homogenization, the addition of Er obviously improves the hardness of the alloys. The strength of the alloys significantly increases when the addition of Er is 0.33 wt.%. The atomic radius of Er is larger than Al. When a small quantity of Er atoms is dissolved into Al lattice, the lattice distortion is produced causing the solid-solution strengthening. The addition of Er also refines the microstructure. Refinement also improves the hardness of the alloy. Secondary Al_3Er and $Al_3(Er, Zr)$ particles disperse uniformly in the matrix with a small size. Fine precipitated particles, to a certain extent, increase the

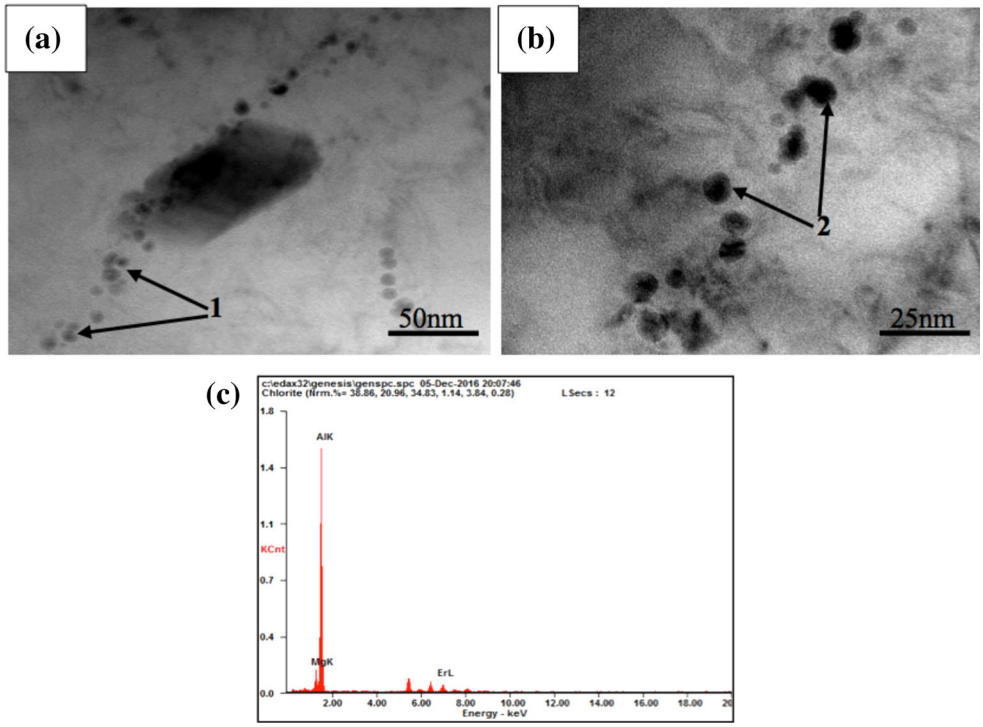

Fig. 7 TEM images and the EDS patterns of the alloy with 0.33 wt.% Er after homogenizing at 490 °C for 24 h: (a) image showing secondary Al_3Er, (b) image showing $Al_3(Er, Zr)$, (c) EDS patterns for the marked particles by arrow 1 in (a)

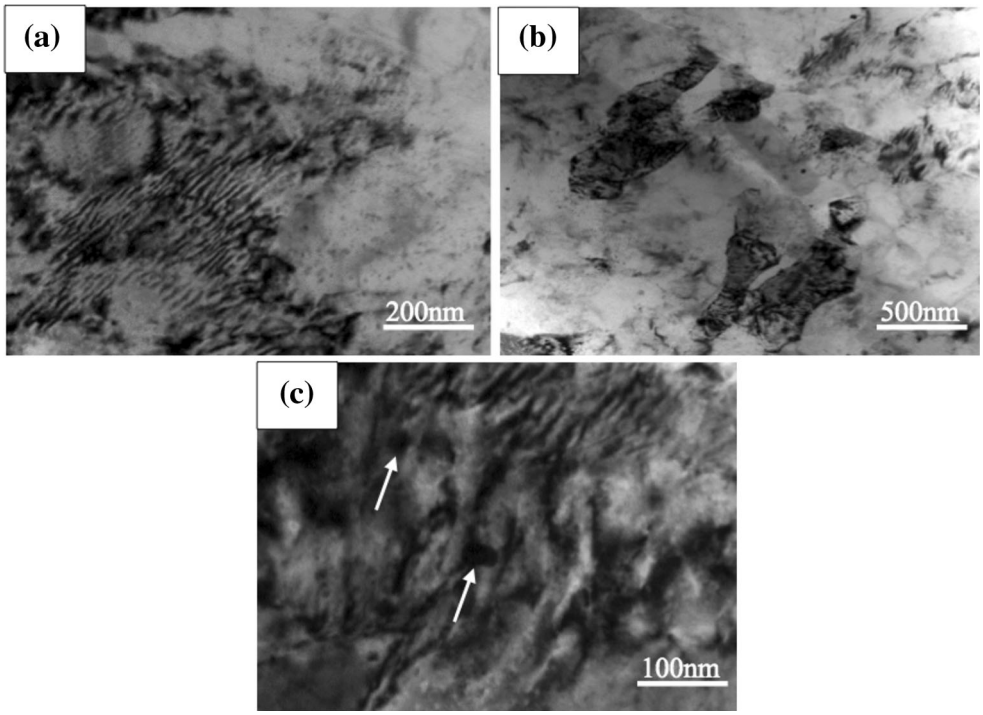

Fig. 8 TEM images of the alloy with 0.33 wt.% Er after annealing at 250 °C for 2 h

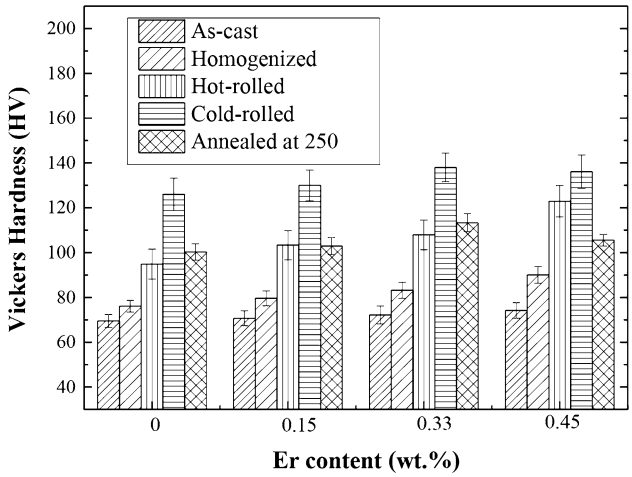

Fig. 9 Hardness of the alloys under different states

Table 2 Tensile properties of the alloys after annealing at 250 °C for 2 h

Alloys	σ_b, MPa	$\sigma_{0.2}$, MPa	δ, %
Al-6.5Mg-0.4Mn-0.1Cr-0.1Zr	431 ± 8	325 ± 9	12.9 ± 0.9
Al-6.5Mg-0.4Mn-0.1Cr-0.1Zr-0.15Er	444 ± 10	346 ± 6	11.2 ± 0.5
Al-6.5Mg-0.4Mn-0.1Cr-0.1Zr-0.33Er	461 ± 5	357 ± 7	10.8 ± 0.9
Al-6.5Mg-0.4Mn-0.1Cr-0.1Zr-0.45Er	445 ± 7	350 ± 8	11.0 ± 0.6

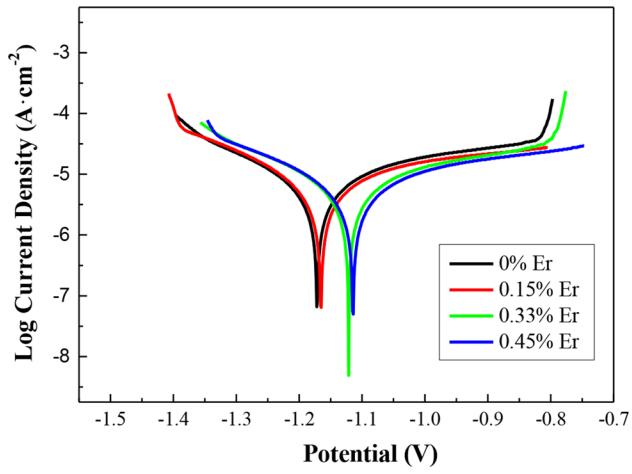

Fig. 10 Tafel polar curves of the alloys annealed at 250 °C for 2 h

hardness of the alloy. Therefore, as for the as-cast and homogenization alloys, the strengthening effect of Er on the alloy can be attributed to solid-solution strengthening, refinement strengthening, and secondary-phase strengthening.

In the process of deformation, a great amount of dislocations entangle together with high density. During the annealing at 250 °C, almost all the dislocations in the alloy get enough energy to move, and the dislocation density decreases due to the interaction between opposite sign dislocations. After hot rolling and cold rolling, secondary Al_3Er and $Al_3(Er,Zr)$ particles are crushed and distribute with a smaller size. During the movement of dislocations, Al_3Er and $Al_3(Er,Zr)$ particles strongly pin up dislocations and sub-boundaries. Accordingly, the strength of the alloy is improved.

Excessive erbium addition deteriorates the mechanical properties of the alloy. This can be explained that the role of primary Al_3Er is mainly to increase constitutional supercooling and provide heterogeneous nucleation. When the Er content is large, the size and amount of Al_3Er both increase, as shown in Fig. 3(d). During deformation process, the coarse eutectic primary Al_3Er may be separated from the matrix and form microcracks, which deteriorates the mechanical properties of the alloy.

With Er addition, the susceptibility of intergranular corrosion is reduced. Er atoms can enter the γ-Al_2O_3 oxide film and form the composite oxide film of Er-O and Al-O, which makes the surface oxide film more compact (Ref 21, 22). The composite oxide film can effectively resist the invasion of Cl^- so that the corrosion resistance is improved (Ref 23). Impurity always accelerates the corrosion rate of aluminum alloy. Er has a strong affinity to the impurity in the alloy. The addition of Er can play a role in purification and modification. The potential of Al_3Er phase is higher than that of Al_6Mn. The addition of Er increases the potential of the precipitated phase, which decreases the trend of corrosion (Ref 24, 25). With the stable Al_3Er and $Al_3(Er, Zr)$ precipitation, the continuous precipitation of Al_3Mg_2 phase is prevented, and the intergranular corrosion susceptibility decreases.

5. Conclusions

1. The primary Al_3Er restricts the growth of dendrites during solidification. The effect of refinement is significant when the addition of Er is 0.33 wt.%. After homogenization, secondary Al_3Er and $Al_3(Er, Zr)$ precipitate from the solid solution.
2. The addition of Er obviously improves mechanical properties. The strengthening can be attributed to solid-solution strengthening due to the dissolving of Er into Al, refinement strengthening caused by constitutional supercooling and heterogeneous nucleation, and secondary-phase strengthening coming from Al_3Er and $Al_3(Er, Zr)$.
3. With the increment of Er content, the corrosion resistance is improved, which can be attributed to the compact composite oxide film of Er-O and Al-O, purification, and modification.

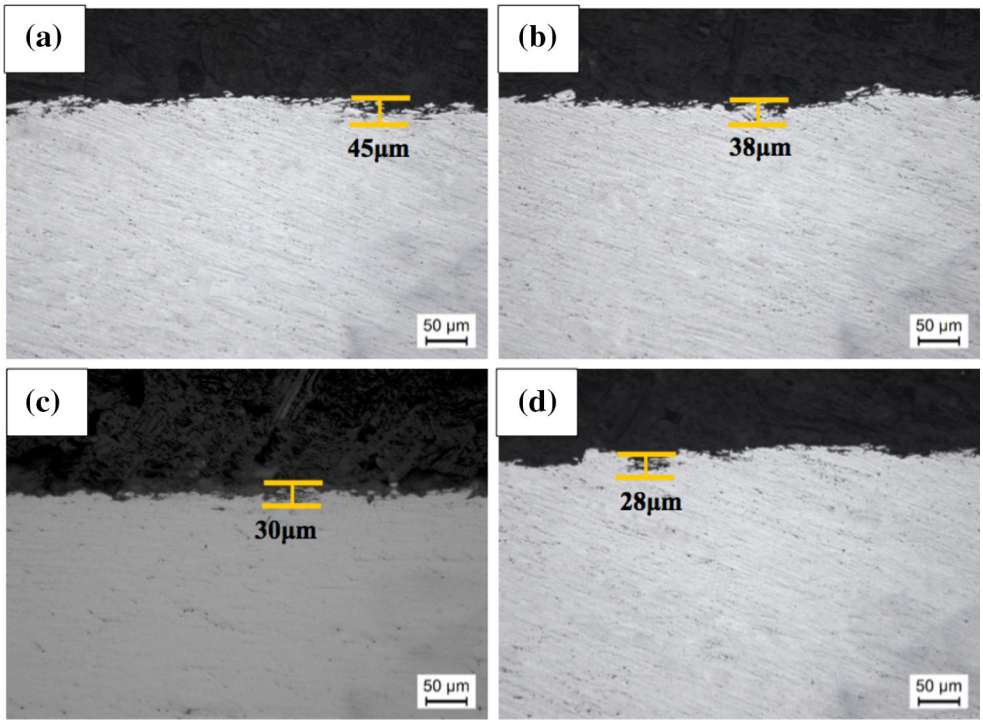

Fig. 11 Typical cross-sectional corrosion morphologies and maximum corrosion depths of the alloys stabilizing annealed at 250 °C (a) without Er, (b) 0.15 wt.% Er, (c) 0.33 wt.% Er, (d) 0.45 wt.% Er

Acknowledgments

This paper was supported by National Natural Science Foundation (51671063, 51771060), Heilongjian Province Natural Science Foundation (ZD2017010), the Fundamental Research Funds for the Central Universities (HEUCFG201834), Harbin City Application Technology Research and Development Project (2015AE4AE005, 2015RQXXJ001, 2016AB2AG013), and Key Laboratory of Lightweight and High Strength Structural Materials of Jiangxi Province (No. 2017BCD40003).

References

1. D.K. Xu, P.A. Rometsch, and N. Birbilis, Improved Solution Treatment for an As-Rolled Al-Zn-Mg-Cu Alloy. Part I. Characterisation of Constituent Particles and Overheating, *Mater. Sci. Eng. A*, 2012, **534**, p 234–243
2. D.K. Xu, P.A. Rometsch, and N. Birbilis, Improved Solution Treatment for an As-Rolled Al-Zn-Mg-Cu Alloy. Part II. Microstructure and Mechanical Properties, *Mater. Sci. Eng. A*, 2012, **534**, p 244–252
3. B.J. Wang, D.K. Xu, J.H. Dong, and W. Ke, Effect of Texture on Biodegradable Behavior of an As-Extruded Mg-3% Al-1% Zn Alloy in Phosphate Buffer Saline Medium, *J. Mater. Sci. Technol.*, 2016, **32**, p 646–652
4. S. Lathabai and P.G. Lloyd, The Effect of Scandium on the Microstructure, Mechanical Properties and Weldability of a Cast Al-Mg Alloy, *Acta Mater.*, 2002, **50**(17), p 4275–4292
5. R.G. Guan, Y.F. Shen, Z.Y. Zhao, and X. Wang, A high-Strength, Ductile Al-0.35Sc-0.2Zr Alloy with Good Electrical Conductivity Strengthened by Coherent Nanosized-Precipitates, *J. Mater. Sci. Technol.*, 2016, **33**, p 215–223
6. A. Medjahed, A. Henniche, M. Derradji, T.F. Yu, Y. Wang, R.Z. Wu, L.G. Hou, J.H. Zhang, X.L. Li, and M.L. Zhang, Effects of Cu/Mg Ratio on the Microstructure, Mechanical and Corrosion Properties of Al-Li-Cu-Mg-X Alloys, *Mater. Sci. Eng. A*, 2018, **718**, p 241–249
7. Y. Wang, Z. Li, T.F. Yu, A. Medjahed, R.Z. Wu, L.G. Hou, J.H. Zhang, X.L. Li, and M.L. Zhang, Effect of Sc and Zr on Microstructure and Mechanical Properties of As-Cast Al-Li-Cu Alloys, *Adv. Eng. Mater.*, 2017, https://doi.org/10.1002/adem.201700898
8. A. Medjahed, H. Moula, A. Zegaoui, M. Derradji, A. Henniche, R.Z. Wu, L.G. Hou, J.H. Zhang, and M.L. Zhang, Influence of the Rolling Direction on the Microstructure, Mechanical, Anisotropy and Gamma Rays Shielding Properties of an Al-Cu-Li-Mg-X Alloy, *Mater. Sci. Eng. A*, 2018, **732**, p 129–137
9. M. Song, K. Du, Z.Y. Huang, H. Huang, and Z.R. Nie, Deformation-Induced Dissolution and Growth of Precipitates in an Al-Mg-Er Alloy During High-Cycle Fatigue, *Acta Mater.*, 2014, **81**, p 409–419
10. H.Y. Li, J. Bin, J.J. Liu, and Z.H. Gao, Synergetic Effect of Er and Zr on the Precipitation Hardening of Al-Er-Zr Alloy, *Scr. Mater.*, 2012, **67**(1), p 73–76
11. D. Zhemchuzhnikova, A. Mogucheva, and R. Kaibyshev, Mechanical Properties and Fracture Behavior of an Al-Mg-Sc-Zr Alloy at Ambient and Subzero Temperatures, *Mater. Sci. Eng. A*, 2013, **565**, p 132–141
12. K.B. Hyde, A.F. Norman, and P.B. Prangnell, The Effect of Cooling Rate on the Morphology of Primary AlSc Intermetallic Particles in Al-Sc Alloys, *Acta Mater.*, 2011, **49**(8), p 1327–1337
13. Y.L. Liu, L. Luo, C.F. Han, L.Y. Ou, J.J. Wang, and C.Z. Liu, Effect of Fe, Si and Cooling Rate on the Formation of Fe- and Mn-Rich Intermetallics in Al-5Mg-0.8Mn Alloy, *J. Mater. Sci. Technol.*, 2015, **32**(4), p 305–312
14. H.Y. Li, Z.H. Gao, H. Yin, H.F. Jiang, X.J. Su, and J. Bin, Effects of Er and Zr Additions on Precipitation and Recrystallization of Pure Aluminum, *Scr. Mater.*, 2013, **68**, p 59–62
15. S.P. Wen, Z.B. Xing, H. Huang, B.L. Li, W. Wang, and Z.R. Nie, The Effect of Erbium on the Microstructure and Mechanical Properties of Al-Mg-Mn-Zr Alloy, *Mater. Sci. Eng. A*, 2009, **56**, p 42–49
16. X.L. Ji, Z.R. Nie, and Z.B. Xing, Effects of Rare Earth Er on As-Cast Microstructure of Al-Mg Alloy, *Light Alloy Fabr. Technol.*, 2005, **33**(10), p 19–21
17. H. Pan, Z. Han, and B. Liu, Study on Dendritic Growth in Pressurized Solidification of Mg-Al Alloy Using Phase Field Simulation, *J. Mater. Sci. Technol.*, 2015, **32**(1), p 68–75

18. M.J. Jones and F.J. Humphreys, Interaction of Recrystallization and Precipitation: the Effect of Al3Sc on the Recrystallization Behaviour of Deformed Aluminium, *Acta Mater.*, 2003, **51**(8), p 2149–2159
19. J.D. Robson, Modelling the Overlap of Nucleation, Growth and Coarsening During Precipitation, *Acta Mater.*, 2004, **52**(15), p 4669–4676
20. Z.H. Gao, H.Y. Li, Y.Q. Lai, Y.X. Ou, and D.W. Li, Effects of Minor Zr and Er on Microstructure and Mechanical Properties of Pure Aluminum, *Mater. Sci. Eng. A*, 2013, **580**(10), p 92–98
21. J. Beretka, M.J. Ridge, Dehydration Products of Aluminium Hydroxides, *J. Chem. Soc. A*, 1967, **6**, p 2106–2109
22. M.X. Gong, L.J. Yan, Y.J. Wang, and H. Du, Study on Seawater Corrosion Resisting Properties of Al-Mg-RE Alloy Gauze, *J. Rare Earth*, 1999, **18**(4), p 248–253
23. S. Jain, M.L.C. Lim, J.L. Hudson, and J.R. Scully, Spreading of Intergranular Corrosion on the Surface of Sensitized Al-4.4Mg Alloys: A General Finding, *Corros. Sci.*, 2012, **59**(3), p 136–147
24. F. Rosalbino, E. Angelini, D.S. Negri, A. Saccone, and S. Delfino, Influence of the Rare Earth Content on the Electrochemical Behaviour of Al-Mg-Er Alloys, *Intermetallics*, 2003, **11**(5), p 435–441
25. Y.S. Ding, The Effect of Mg Content on Intergranular Corrosion of Al-Mg-Mn Alloys After Annealing, *Mater. Sci. Forum*, 2016, **877**, p 514–521